Inhibition of Jahn−Teller Cooperative Distortion in $LiMn_2O_4$ Spinel by Ga^{3+} Doping

Doretta Capsoni,[†] Marcella Bini,[†] Gaetano Chiodelli,[†] Piercarlo Mustarelli,[†,‡] Vincenzo Massarotti,*[,†] Carlo B. Azzoni,[‡] Maria C. Mozzati,[‡] and Laura Linati[§]

Dipartimento di Chimica Fisica "M. Rolla" and CSTE-CNR, Università di Pavia, via Taramelli 16, I-27100 Pavia, Italia, INFM−Dipartimento di Fisica "Alessandro Volta", Università di Pavia, via Bassi 6, I-27100 Pavia, Italy, and Centro Grandi Strumenti, Università di Pavia, Via Bassi 21, I-27100 Pavia, Italia

Received: January 23, 2002; In Final Form: May 14, 2002

Ga-doped Li−Mn-spinels $Li_{1.02}Ga_xMn_{1.98-x}O_4$ with $0.00 \le x \le 0.20$ are investigated to verify the lattice capability to allocate the Ga^{3+} ions on both tetrahedral and octahedral sites and to determine the lowest amount of dopant that prevents the occurrence of the Jahn−Teller (J−T) transition observed near room temperature in $LiMn_2O_4$. XRPD, NMR, and EPR spectra and static magnetic susceptibility and conductivity data are related to the site occupancy, the Mn valence state and the homogeneous distribution of the dopant. The electronic and magnetic features of the spinel framework are strongly dependent on substitution in its cationic sublattice: dopant amounts as low as 1% significantly modify the temperature of the conductivity drop associated with the J−T distortion. Ga^{3+} ions substitute chiefly in the octahedral sites, Mn^{4+} ions occupy regular and distorted octahedral sites and, at the same time, the value of lattice parameter remains unchanged. Mn^{2+} ions are present in the tetrahedral site and Li^+ increases in the octahedral site as a consequence of Li−Mn/Ga inversion. Such a mechanism increases the efficiency of J−T inhibition by Ga doping, in comparison with transition cations having the same valence.

1. Introduction

The $LiMn_2O_4$ spinel is a very useful cathode material employed in rechargeable lithium batteries for electrical vehicles and for microelectronic devices.[1] The close-packed oxygen array may allocate cations in tetrahedral and octahedral sites to build up the spinel structure. Other sites unoccupied by cations are suitable for Li insertion/emptying in charge/discharge processes of a battery. In the stoichiometric spinel the same amount of Mn^{3+} and Mn^{4+} occupies the 16d octahedral position and a Jahn−Teller (J−T) cooperative distortion of the $Mn^{3+}O_6$ octahedra produces a cubic-to-orthorhombic transition around room temperature (rt)[2,3] that changes the charge/discharge features and affects the cathode stability. For this reason, to achieve a long battery life and good performance at the working temperature, it is important to avoid the J−T transition. A suitable increase of the ratio $r = |Mn^{4+}|/|Mn^{3+}|$, by lithium excess (y)[4] or by cation doping (x), can avoid the J−T transition. A spinel phase with a lithium excess gave evidence of Li substitution in octahedral sites[5] according to the formula $[Li^+]_{tetra}[Li^+_yMn^{3+}_{1-3y}\ Mn^{4+}_{1+2y}]_{octa}O_4$.

As we demonstrated in a previous work,[6] by replacement of a trivalent M^{3+} transition ion (Co, Cr) according to the charge distribution $[Li^+_{1-y}]_{tetra}[Li^+_yM^{3+}_xMn^{3+}_{1-3y-x}Mn^{4+}_{1+2y}]_{octa}$ with $y = 0.02$, the stabilization of cubic symmetry in the 16d site is already achieved for $x = 0.06$ and, consequently, $r = 1.18$. The same r value was also found to hold in the case of substitution with Ni^{2+}, for which there is no J−T distortion with $x = 0.02$ according to its pertinent charge distribution.[6] A similar effect on J−T distortion could be found by substituting suitable nontransition cations having a unique valence state, such as Ga^{3+}, Al^{3+}, and Mg^{2+}. At the same time, it would be interesting to know the capability of the same ions to distribute between 16d and 8a cationic sites, giving possibly a different influence on the J−T effect. The Ga^{3+} ion can substitute on both spinel sites,[7] and moreover, its distribution on the cationic sublattice could be checked by the ^{71}Ga NMR probe.

In this paper we analyze the behavior of Li−Mn spinels doped with the trivalent cation Ga^{3+}. X-ray powder diffraction (XRPD), nuclear magnetic resonance (NMR), electron paramagnetic resonance (EPR), and magnetic susceptibility measurements are performed to verify the homogeneous dilution of Ga^{3+}, its distribution on the octahedral and tetrahedral sites, the Mn valence state, and the possible formation of spurious phases. Sensitive tests of the J−T distortion are provided by XRPD and conductivity measurements as a function of the temperature. We stress here that our main goal remains the inhibition of the J−T cooperative distortion near the working temperature with the minimum amount of substitution to improve both capacity and lifetime of the Li batteries employing this cathode material.

2. Experimental Section

Samples Preparation. Ga-doped samples were prepared by reacting MnO_2 with $Ga(NO_3)_3{\cdot}9H_2O$ and $LiOH{\cdot}H_2O$[7] in the amount required to obtain the composition $Li_{1.02}Ga_xMn_{1.98-x}O_4$ with $0.00 < x \le 0.20$. The first heating step was performed at 773 K; then the samples were brought to rt, ground, heated to 1073 K at 5 K/min, and annealed for 8 h in air several times to reach homogeneous composition, as checked by EPR and XRPD. For conductivity measurements, the powder was pressed in the form of bars and sintered at 1073 K in air for 10 h. For comparison, a $x = 0.00$ sample previously prepared[6] is reported.

Apparatus and Procedures. The XRPD patterns have been collected with a Bruker D5005 diffractometer (Cu Kα radiation,

* Corresponding author. Fax: +39 0382 507575. E-mail vimas@chifis.unipv.it.
[†] Dipartimento di Chimica Fisica "M. Rolla" and CSTE-CNR.
[‡] INFM−Dipartimento di Fisica "Alessandro Volta".
[§] Centro Grandi Strumenti, Università di Pavia.

10.1021/jp020220u CCC: $22.00
Published on Web 07/03/2002

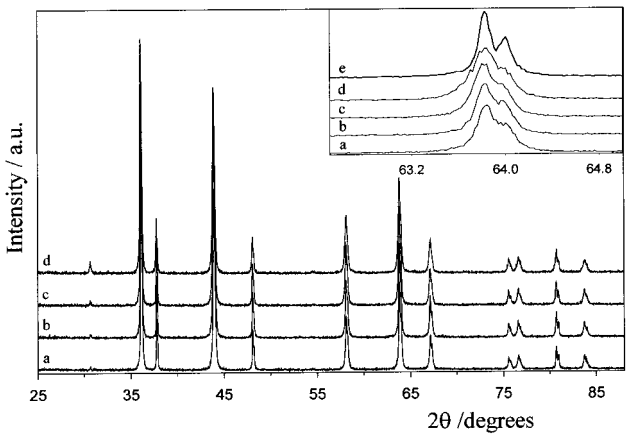

Figure 1. XRPD patterns at rt of (a) $x = 0.02$, (b) $x = 0.04$, (c) $x = 0.06$, and (d) $x = 0.20$ samples. The inset shows the 440 reflection of the same patterns compared with the (e) $x = 0.00$ sample.

Bragg−Brentano geometry) equipped with a $\theta-\theta$ goniometer and curved graphite monochromator on the diffracted beam. The explored temperature range is $100 \leq T/K \leq 333$ on cooling and heating by a TTK450 Anton Paar polythermal equipment. The rt patterns have been collected in the $15 \leq 2\theta/deg \leq 130$ angular range, with steps of 0.02° and 8 s counting time per step. To investigate the presence of J−T transition, XRPD data were collected at different temperatures in the $37.3 \leq 2\theta/deg \leq 38.5$ and $63 \leq 2\theta/deg \leq 65$ angular ranges, where the 222 and 440 cubic reflections respectively are present. The structural and profile Rietveld analyses have been carried out with the FULLPROF program.[8]

EPR measurements in the X band (~9.5 GHz) were performed with a Bruker spectrometer with a continuous nitrogen flow apparatus to study the temperature dependence in the range 150−500 K.

Static magnetization was measured from 300 K down to 2 K with a SQUID magnetometer (Quantum Design).

The system for conductivity measurements has been described elsewhere.[5]

The NMR measurements were performed on a AMX400WB spectrometer (Bruker) based on a 9.4-T magnet. ^{7}Li static and MAS (magic angle spinning) measurements were performed at 155.6 MHz with a 4 mm CP-MAS probe (Bruker). Spinning speeds from 6 to 13 kHz were employed. A single-pulse sequence was used with a pulse width of 0.5 μs, corresponding to a tip angle of ~30°. The free induction decay (FID) signals were left-shifted and Fourier transformed without line broadening. The spectra were referenced to an external sample of 1.0 M LiCl in H_2O. ^{71}Ga spectra were acquired at the frequency of 121.98 MHz with a 4 mm CP-MAS probe (Bruker). The spectra were averaged over 24k acquisitions. A single pulse sequence (pulse width 6 μs) was used. We did not see significant differences between the spectra in static conditions and those acquired under MAS rotation. A recycle time of 0.2 s was employed. The spectra were referenced to $Ga(NO_3)_3$ saturated solution.

3. Results

3.1. XRPD. The diffraction patterns at rt of the doped samples are shown in Figure 1. The $0 < x \leq 0.06$ samples display only the cubic spinel phase. The peak positions are in good agreement with those of the pure spinel. The sample $x = 0.20$ shows small amounts (<1%) of Li_2MnO_3 and $LiGaO_2$; moreover, at $2\theta \approx 30°$ the 220 spinel reflection increases its intensity, suggesting the substitution of Mn and/or Ga ion on the tetrahedral (8a) site.[7,9] A significant line broadening (see inset of Figure 1) is observed with respect to the pure sample, indicating the little particle size related to the peculiar synthesis from nitrates.

TABLE 1

x	0.02	0.04	0.06	0.20
a/Å	8.2399(1)	8.2394(1)	8.2396(1)	8.2400(1)
8a site:Li	0.988(5)	0.985(5)	0.974(5)	0.899(4)
Mn	0.012(5)	0.015(5)	0.026(5)	0.101(4)
16d site:Mn	1.948(5)	1.925(5)	1.901(5)	1.687(4)
Li	0.032(5)	0.035(5)	0.039(5)	0.113(4)
R_p	22.7	22.0	21.0	21.4
R_{wp}	23.4	23.3	22.0	21.7
S	1.15	1.20	1.16	1.15

The lattice parameter values reported in Table 1 were obtained through Rietveld refinement performed on the basis of the cubic $LiMn_2O_4$ structural model. The a values are independent of x. Satisfactory results were obtained by inserting Mn and/or Ga on the 8a site. Due to their similar X-ray scattering powers, it is difficult to assess the real Mn and Ga distribution in the cationic sublattice: the ions in fact have a very similar influence on the electron density of the substituted site. The cationic distribution reported in Table 1 has been obtained by allowing the presence of Mn in the 8a site, whereas Ga ions are fixed on the 16d site. Similar results were obtained by allowing Ga to distribute on both 8a and 16d sites. The reliability of results obtained by the Rietveld refinement are confirmed by satisfactory values of discrepancy factors R_p and R_{wp} and of goodness of fit S,[8] reported in Table 1.

Diffraction patterns taken at different temperatures can also reveal the structural change from the cubic to the orthorhombic cell that, in the angular region of the cubic 222 and 440 reflections, gives rise to three (662 strong; 153 and 513 very weak) and seven (12,12,0, 0,12,4 and 12,0,4 strong; 375, 735, 2,12,4 and 12,2,4 very weak) reflections, respectively.[3] It is expected that the 222 reflection is not influenced by the transition, while the 440 splits into three evident peaks. For the $x = 0.02$ sample, the 440 cubic line splits between 243 and 213 K when T decreases (see Figure 2a); on heating, this splitting disappears between 228 and 243 K. Figure 2b shows the temperature trend of the position of the 440 and those of the three most intense reflections for the orthorhombic cell. Figure 2b also shows that the cubic 222 line, as expected, does not display evident splitting at any temperature in the observation range. The J−T transition temperature is remarkably lower with respect to the undoped spinel.[3]

For the $x = 0.04$ sample no splitting is observed for the 440 reflection over the whole temperature range. A single peak satisfactorily fits the experimental data; its position is shown in Figure 3a as a function of T. A significant reversible increase of the peak broadening is observed between 213 and 133 K. The same trend is not evidenced for the 222 peak. The full width at half-maximum (fwhm) of both reflections is shown in Figure 3b.

For the $x = 0.06$ sample a temperature trend of position and broadening of peaks similar to $x = 0.04$ is observed. These results are shown in Figure 4a,b: the fwhm of the 440 reflection is quite constant between 300 and 173 K, while a slight broadening is observed for $T < 173$ K.

3.2. dc Conductivity. dc conductivity data, expressed as log(σ) vs T, are reported in Figure 5a,b. The drop in conductivity observed near rt in the $x = 0.00$ sample, related to the cubic−orthorhombic transition,[2,3] is no longer present in the doped samples. In the $x = 0.02$ sample a small hysteretic cycle can be observed between 240 and 263 K. A similar effect, though

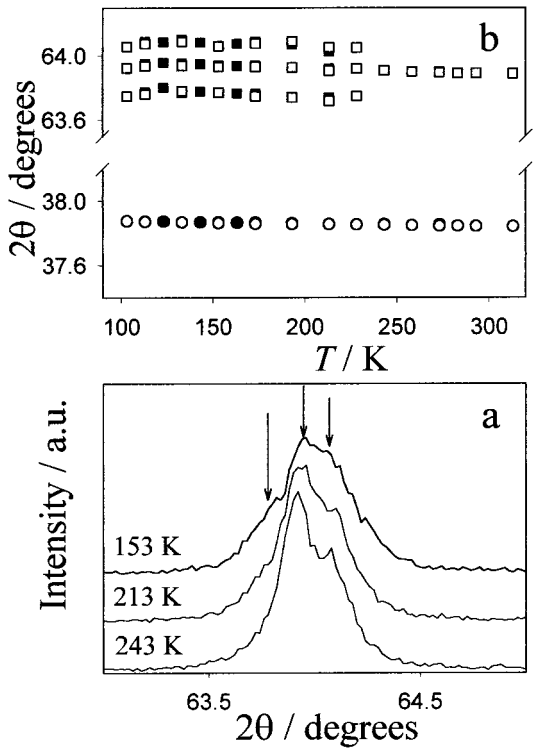

Figure 2. (a) XRPD patterns on cooling of the $x = 0.02$ sample collected at the reported temperatures to show the cubic−orthorhombic transition. The arrows indicate the position of the three strongest orthorhombic peaks. (b) Position of the fitted peaks for the cubic 222 (circles) and 440 (squares) reflections as a function of temperature on cooling (filled symbols) and on heating (empty symbols).

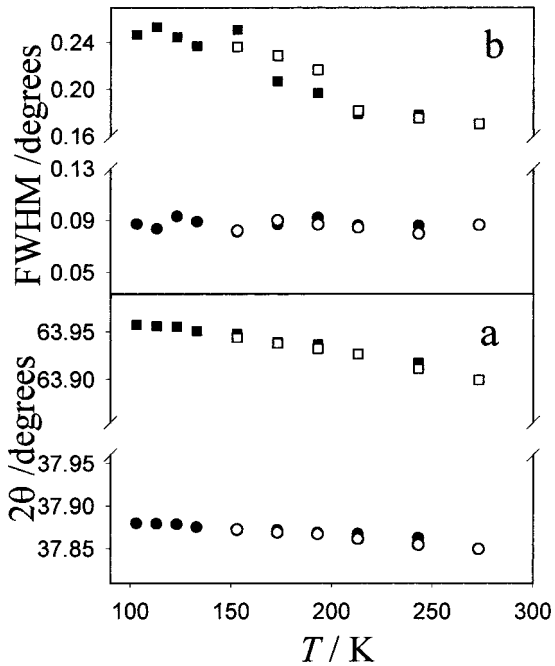

Figure 3. (a) Peak position and (b) fwhm of the 222 (circles) and 440 (squares) reflections as a function of T on cooling (filled symbols) and on heating (empty symbols) for $x = 0.04$ sample.

less evident, is observed over a similar temperature range for the $x = 0.04$ sample. Besides, a slight change of conductivity with an anomalous behavior is evident for $T > 285$ K in the $x = 0.02$ and 0.04 samples: the conductivity is higher on heating than on cooling. At the end of the cooling−heating process, isothermal measurements at 310 K showed a gradual decrease

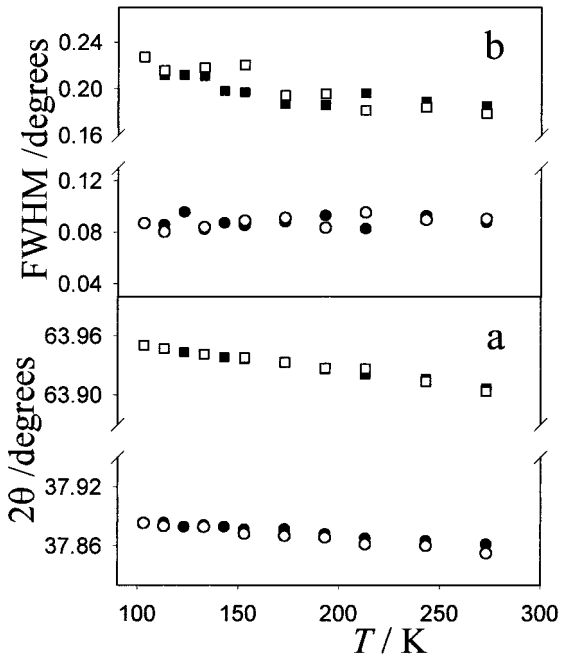

Figure 4. (a) Peak position and (b) fwhm of the 222 (circles) and 440 (squares) reflections as a function of T on cooling (filled symbols) and on heating (empty symbols) for $x = 0.06$ sample.

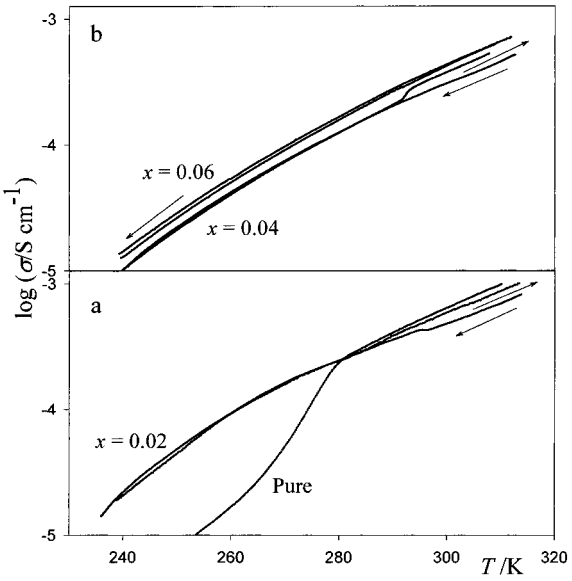

Figure 5. log(σ) as a function of T of (a) $x = 0.00$ and 0.02 and (b) $x = 0.04$ and 0.06 samples. Arrows indicate the cooling and heating process.

of conductivity as a function of time, reaching in a matter of several hours the values recorded at the beginning of the thermal cycle.

3.3. EPR and Magnetic Susceptibility Measurements. In Figure 6 the rt EPR spectra of the doped samples are compared with the $Li_{1.02}Mn_{1.98}O_4$ signal. All the spectra are mainly due to a broad signal (signal A) with a line width $\Delta B \approx 3000$ G and a spectroscopic factor $g \approx 2$, very similar to that of the pure spinel. A signal (B) with a resonant field at about 2000−2500 G is evident in the $x = 0.06$ and 0.20 samples. Another signal (C) with $\Delta B \approx 200$ G centered at $g = 1.994$ is present in the spectra of the 0.02, 0.04, and 0.20 samples. These signals were previously observed in transition cation doped spinels[6] and attributed as follows: A, to the pure spinel phase; B, to Mn^{4+} ions in low symmetry cationic sites, probably in the grain

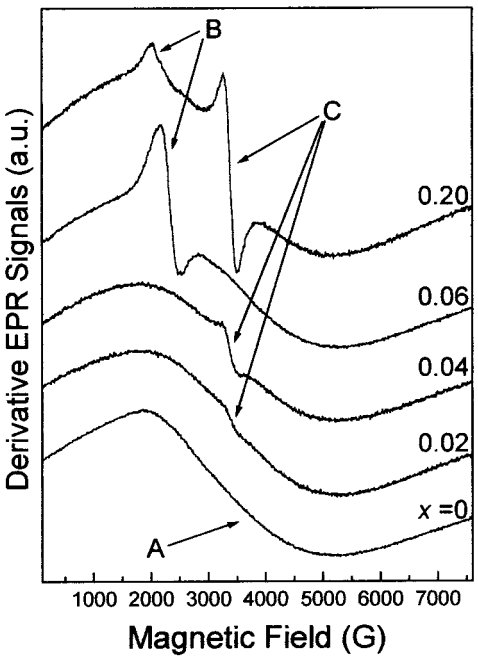

Figure 6. EPR spectra at rt of pure and doped samples. Signal components A−C are indicated.

boundary; C, to the Li_2MnO_3 phase. The amount of such phase is roughly estimated to be less than few percent in the $x = 0.20$ sample.

Figure 7 shows the EPR spectra for $T <$ rt for samples with $x \leq 0.06$. Several different signals appear at $T \leq 263$ K for the 0.02 sample and at $T \leq 243$ K for the 0.04 sample. With decreasing T, these signals merge into only one signal with a resonant field of about 2000−2500 G, i.e., in the same region of the signal B observed for the 0.06 sample. In the case of $x = 0.06$, signal B is observed over the whole investigated temperature range and simply broadens with decreasing T. Finally, signal C, observed in the $x = 0.02$ and 0.04 samples, decreases with T.

Figure 8 shows the comparison between the reciprocal magnetic susceptibility of the $x = 0.02$ sample and the pure spinel. Both field cooling (FC) and zero field cooling (ZFC) curves at 1 kG are reported.

3.4. NMR. Figure 9 shows the ^{7}Li MAS NMR spectra. In general, the ^{7}Li MAS spectra of Mn-containing paramagnetic spinels are well-known to span over thousands of ppm[10,11] and to be characterized by complex spinning sideband manifolds due to the modulation of the anisotropy part of the electron−nucleus dipolar interaction.[12] The isotropic shift is of the order of several hundred ppm and it is due to Fermi contact.[10]

The spectrum of the $x = 0.02$ sample displays a narrow and intense peak at 539 ppm, attributed to the lithium in the 8a spinel site, and a modulation at ∼850 ppm that, in principle, can be due to one or both of the following contributions: (i) Li in a site of a minority-phase-like Li_2MnO_3;[10] (ii) Li in the 16d spinel site, because of the small lithium excess adopted in the sample preparation, or of an inversion process that brings Ga and/or Mn on the 8a site (see Figure 1 and Table 1). We can rule out contribution i, because the Li_2MnO_3 phase was not observed by EPR in sample $x = 0.06$, which shows a ^{7}Li spectrum very similar to the other samples. Therefore, we assign the observed modulation to octahedrally coordinated lithium belonging to the spinel phase. In this case, a shift of ∼850 ppm for the 16d crystallographic position may be justified by considering that this site is connected via 12 Li−O−Mn bonds at ∼90° to 6

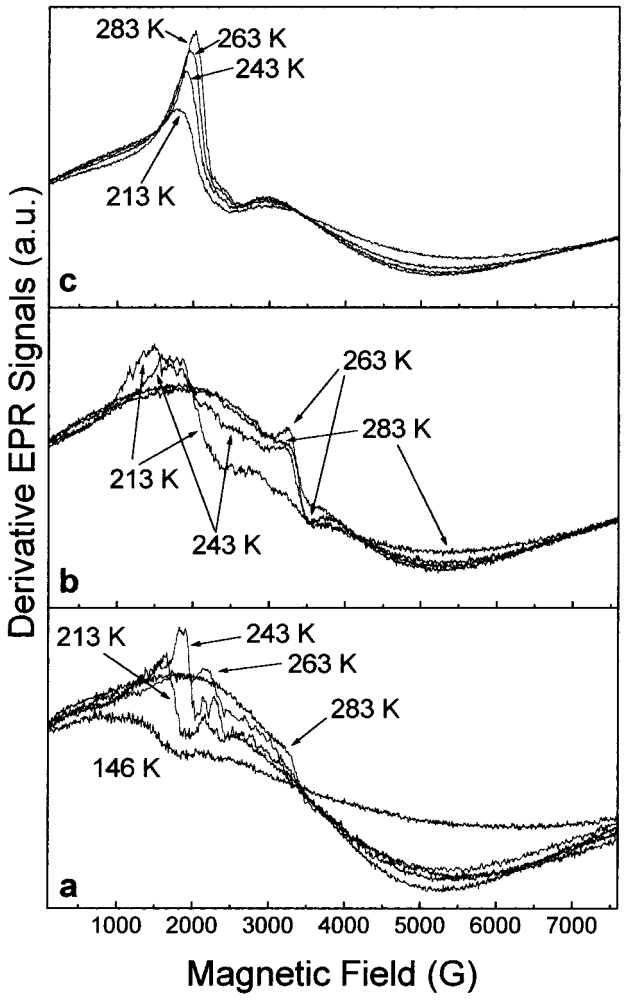

Figure 7. EPR spectra at different temperatures of (a) $x = 0.02$, (b) $x = 0.04$, and (c) $x = 0.06$ samples.

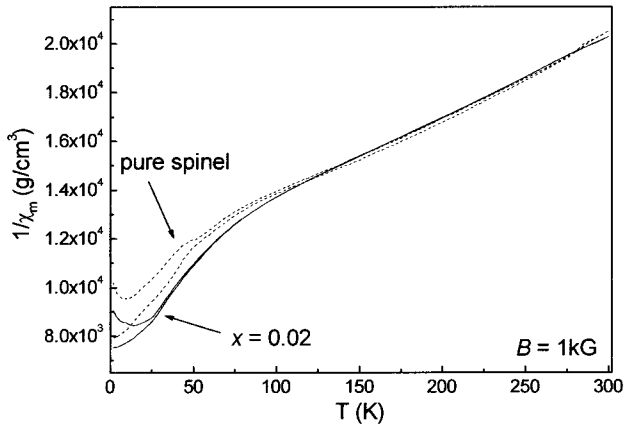

Figure 8. Reciprocal magnetic susceptibility of pure and doped ($x = 0.02$) samples. FC and ZFC curves are shown.

Mn atoms with an average oxidation number of 3.5 (i.e., 3 Mn^{3+} and 3 Mn^{4+}). Now, it was shown[11] that each Mn^{4+} accounts for ∼300 ppm of paramagnetic shift, whereas the contribution of Mn^{3+} is almost negligible, which roughly gives a net shift around 800−900 ppm. Further support to this assignment is given by the consideration that the 16d position is structurally similar to the octahedral 2b site of Li_2MnO_3, which was referred to fall at 1770 ppm;[10] since all 6 Mn atoms in Li_2MnO_3 do have an oxidation number of 4, a 100% shift increase with respect to that of the spinel is reasonable.

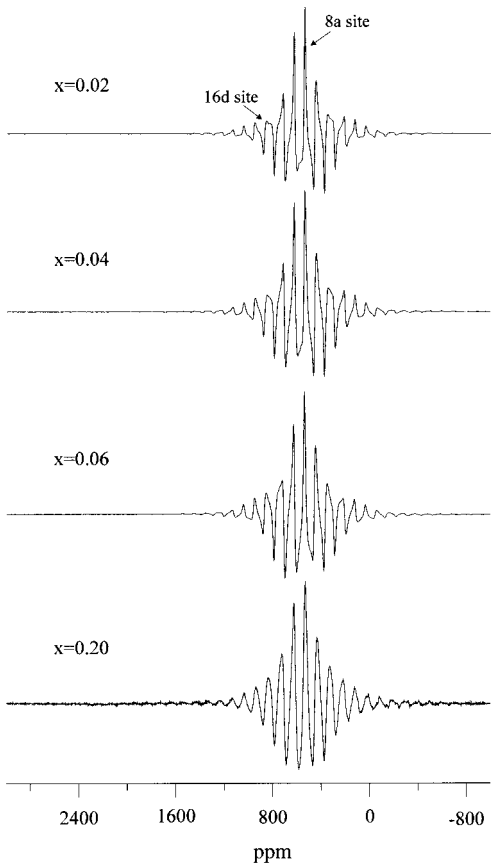

Figure 9. ^{7}Li MAS NMR spectra of the $x = 0.02$, 0.04, 0.06, and 0.20 samples.

The spectra of the $x = 0.04$ and 0.06 samples are very similar to the previous one, but for a progressive increase of the Li population in octahedral sites. The spectrum of sample $x = 0.20$ shows, (i) at very low fields (~1700 ppm), the growth of the signal of lithium in the 2b site[10] of the phase Li_2MnO_3, in agreement with the EPR and XRPD results, and (ii) a broadening of the peaks that can be attributed to the increase of the Li_2MnO_3 phase and the subsequent higher disorder. Finally, a feature is observed near 0 ppm that can be attributed to the diamagnetic compound $LiGaO_2$, a small quantity of which has been revealed by XRPD.

The NMR spectra of ^{71}Ga (nuclear spin $I = {}^3/_2$) are affected by strong quadrupolar broadening that arises from the interaction of the nuclear quadrupolar momentum with the electric field gradient tensor **V** (principal components V_{xx}, V_{yy}, V_{zz}) at the nucleus position. The group of Massiot[13] has recently published a good review on ^{71}Ga solid-state NMR. In the case of moderate quadrupolar coupling (less than few megahertz), they showed that it is possible to obtain resolved spectra also under simple MAS conditions, and to separate the contributions of Ga in tetrahedral and octahedral coordination. Figure 10 shows the ^{71}Ga MAS NMR spectra of the samples $x = 0.04$, 0.06, and 0.20. The spectrum of $x = 0.04$ (very similar to $x = 0.02$) seems to be characterized by the presence of two spin populations: (1) one centered near 0 ppm with an asymmetry parameter $\eta = |V_{xx} - V_{yy}|/V_{zz} \sim 1$ and (2) one with two singularities whose asymmetry can be estimated to be on the order of 0.5. The spectrum of $x = 0.06$, in contrast, seems to be characterized by the presence of a single population whose quadrupolar parameters resemble those of population 2 reported for sample $x = 0.04$. Of course, we cannot exclude that the spectral shape of $x = 0.06$ is due to the increase of population 1 with respect to population 2. Finally, the spectrum of $x = 0.20$ seems to display the growth of population 1 with respect to population 2. We can tentatively assign population 1 to Ga in octahedral sites and, consequently, population 2 to Ga in tetrahedral coordination.

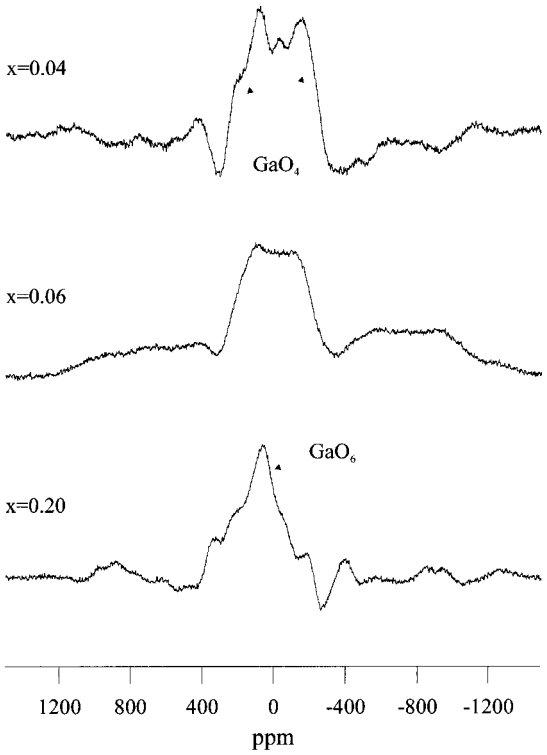

Figure 10. ^{71}Ga NMR spectra of the $x = 0.04$, 0.06, and 0.20 samples.

4. Discussion

The EPR signal A is the most important component of the spectra for all the samples, proving the good dopant dilution and homogeneity of the spinel phase, as widely discussed.[14] Besides, this signal does not depend on x (Figure 6) as also observed for the lattice parameter a by XRPD results.

In a previous work[6] we treated the possible substitution of transition cations on the 16d site, and the charge balance was limited to the pertinent sublattice. The effective replacement of Mn by Ni was checked by neutron diffraction for $x \geq 0.04$.[15]

Now we must consider both the tetrahedral and octahedral sites for possible cation substitution (fractions x_t and x_o, respectively, with $x = x_o + x_t$). The charge balance should be extended to the whole cationic sublattice and the charge distribution becomes

$$[Li^{+}_{1-x_t}Ga^{3+}_{x_t}]_{tetr}[Li^{+}_{y+x_t}Ga^{3+}_{x_o}Mn^{3+}_{1-3y-x}Mn^{4+}_{1+2y}]_{octa} \quad (1)$$

Independent of x_t and x_o fractions on the different cationic sites, the Mn^{3+} decrease depends only on the total substituted amount x. The above-reported distribution agrees with a model of stoichiometric reaction, taking into account the formation of the only spinel phase. According to this charge distribution, for $x = 0.02$ we obtain $r = |Mn^{4+}|/|Mn^{3+}| = 1.13$, a value for which the J−T distortion near rt should be observed, on the basis of the data previously reported for doping with transition cations.[6] However, conductivity data show no evidence of σ drop near rt, and the hysteretic loop observed between 240 and 263 K (see Figure 5) is in agreement with the low-temperature XRPD data, showing the cubic−orthorhombic transition for 213

$K < T < 243$ K (see Figure 2). In addition, the magnetic susceptibility data reported in Figure 8 show very little difference with respect to the pure spinel, except for the absence of the slope change near rt due to the J−T transition. A more effective distribution model that could explain the absence of the J−T effect near rt in sample $x = 0.02$ is

$$[Li^{+}_{1-z}Mn^{2+}_{z}]_{tetr}[Li^{+}_{y+z}Ga^{3+}_{x}Mn^{3+}_{1-3y-x-2z}Mn^{4+}_{1+2y+z}]_{octa} \quad (2)$$

where the 2^+ oxidation state is evidenced for Mn on the 8a site[9] due to a partial inversion between Mn and Li ions. This fact produces an additional decrease of Mn^{3+} $(-2z)$ and an increase of Mn^{4+} $(+z)$ on the 16d site with respect to the distribution model (1). Now, with $r = (1 + 2y + z)/(1 - 3y - x - 2z)$, the $r = 1.18$ limit value[6] may be reached for $x = 0.02$ and $y = 0.02$ if $z = 0.0136 \approx (2/3)x$. This result agrees with XRPD refined value reported in Table 1 for Mn in the 8a site and does not disagree with EPR signals because Mn^{2+} ($3d^5$ ion) in the intermediate crystal field in tetrahedral coordination shows the same values of the g factor as in octahedral coordination ($g \cong 2$, or slightly greater).[4] This signal is very similar to that observed in the stoichiometric spinel and would not be discernible from that arising from Mn^{4+} ions in octahedral sites, as reported in detail in ref 4.

A more complex model assuming both Ga and Mn on the 8a site could also be proposed to explain the J−T transition inhibition. Indeed, the presence of Mn and/or Ga ions on the tetrahedral site increases the electron density, affecting the 220 reflection intensity, which increases with increasing x, as shown in Figure 1. This effect agrees with that proposed by Yoshio et al.,[7] even if they attributed the 220 increase to the presence of Ga only in the 8a site, and specifically about one-third of the total dopant Ga^{3+}. Due to the similar X-ray scattering power of Ga and Mn, both possibilities may be taken into account and XRPD measurements cannot resolve this doubt. Indeed, a recent neutron diffraction study[16] gives evidence for a total occupancy of octahedral site by Ga. This is in agreement with our charge distribution model (2). On the other hand, also the discrepancy factors and χ^2 values of neutron diffraction refinements[16] should not completely rule out a partial Ga occupancy of the tetrahedral site.

Further information can be obtained from the ^{71}Ga NMR spectra. Figure 10 shows that the higher the Ga content, the higher is the peak we assigned to Ga in the octahedral site. Our NMR results do not allow a simple quantitative estimation of the different spin populations; however we can conclude that Ga is present both in octahedral and tetrahedral sites, and that its "affinity" for the 16d site does increase with its content in the spinel phase. This agrees with the findings of Bellitto et al.[16] and Yoshio et al.[7]

As expected on the basis of distribution model (2), the $x = 0.04$ and 0.06 samples do not show any conductivity drop pertinent to J−T distortion in the examined T range (Figure 5b). On the other hand, the XRPD results show no evident splitting but only a peak broadening for $T < 210$ K in the $x = 0.04$ sample (Figure 3b) and a less evident broadening below 140 K in the $x = 0.06$ sample (Figure 4b).

Our charge distribution model (2) also justifies a rapid increase with x of Mn^{4+} ions, which, if in distorted octahedra, give rise to the EPR signal B present in all the samples at the lowest investigated temperature. With increasing T the signal B spreads into different signals that disappear at $T \geq 263$ K for $x = 0.02$ (Figure 7a) and at $T \geq 243$ K for $x = 0.04$ (Figure 7b) while signal C increases. These dynamical effects suggest variations in the local symmetry around Mn^{4+} ions as a function of T. Some octahedral Mn^{4+} ions in $LiMn_2O_4$ or Li_2MnO_3, respectively, experience a progressive site deformation when the temperature is lowered below a limiting value. At even lower temperatures these deformations become homogeneous and a unique B signal arises. This is particularly evident in the $x = 0.02$ sample at the lowest reported temperature (146 K). This process is reversible and independent of the thermal history of the sample. Similar processes were previously observed for $T > 300$ K in samples doped with transition cations.[6] For $x = 0.06$ this dynamical process is absent: the signal B maintains its shape independent of T (Figure 7c), except for a broadening with decreasing T, and the signal C is never observed in the same T region. This fact suggests an increased thermal stability of the Mn^{4+} environment with respect to the less doped samples. For the $x = 0.02$ and 0.04 samples, the lattice instability and disorder affect also the dc electrical measurements, which show hysteretic cycles in the same temperature range. We can attribute these changes in conductivity to a fraction of charge carriers (assumed to be negative[5]) that become available for the long-range transport only at a given temperature. Indeed, because of a partial occupation of the 8a site by Mn and/or Ga, a fraction of Li atoms is moved to the octahedral site and a shift, ΔE, of the energy levels of the e_g orbitals of the neighboring Mn atoms can occur. As a consequence, the e_g-e_g electron hopping will be locally forbidden and the spinel will experience a partial "electronic crystallization" (Wigner crystallization[17]) due to Coulomb interactions: this will lead to the formation of Mn^{4+} ions in distorted sites, giving rise to the EPR signal B. Such a mechanism was thoroughly discussed in a recent paper,[11] to interpret the behavior vs temperature of ^6Li and ^7Li NMR spectra of defective spinels.

For $kT \cong \Delta E$ the electron hopping starts to take place again, so determining small changes of the dc conductivity, which are evident chiefly for sample $x = 0.02$ (see Figure 5); the network then dynamically rearranges and the signal B disappears. We can also infer that the Wigner crystallization we are discussing is a sort of cooperative process, and that its removal is related to the Ga content. In fact, for $x = 0.06$, the EPR signal B is observed all over the temperature range we examined and, consequently, we do not see any conductivity anomaly.

Finally, the $x = 0.02$ and 0.04 samples display a further anomalous effect in conductivity at ∼290 K, for which we have no corresponding evidence from XRPD and EPR results. The lack of information from our diffractometric and spectroscopic techniques points toward a mechanical relaxation related to the microstructure of the bars pressed for the dc conductivity measurements. We stress here that the reproducibility of the conductivity data has been repeatedly checked.

5. Conclusions

This study shows that in the Ga-substituted spinels the formation of a partially inverted lithium manganese spinel occurs with Mn^{2+} and/or Ga^{3+} in tetrahedral sites, in agreement with our evidence of electron density increase and with neutron powder diffraction results.[16] The presence of Ga^{3+} on both 8a and 16d sites was revealed by ^{71}Ga NMR spectra, while that of Li^+ in 16d sites by ^7Li NMR data. A complex variation of cation species and charge distribution in the cation sublattices inhibits the cooperative cubic−orthorhombic transition, even with a substitution of a small fraction ($x = 0.02$) of Ga^{3+} ions. We showed that, due to the different charge distribution model (2) and pertinent cationic charge distribution, Ga doping acts in a more efficient way with respect to the analogous trivalent

transition cations for which the distribution model (1) (case of $x_t = 0.00$) can be applied. Besides, after Ga substitution, Mn^{4+} ions can occupy both regular and distorted octahedra. Hence, the absence of the J−T effect may be partly due to the nonhomogeneous distribution revealed by the EPR and XRPD results. Detailed analysis of EPR and conductivity data as a function of temperature allowed us to correlate the presence of Mn^{4+} in distorted octahedra (signal B) with hysteresis loops in conductivity pertinent to carriers (electron) localization.

In addition, it was possible to observe a sensible increase of the electronic conductivity below rt in Ga-doped samples with respect to the pure one. High conductivity and structural stability are two of the main requirements for electrochemical applications of Li,Mn spinels as cathode materials.[1,18,19] Besides, according to the literature[20,21] the de-lithiation process is impaired in highly doped samples. This is why it is of practical interest to know the minimum x value that prevents the J−T transition near rt.

Acknowledgment. This work has been partially supported by "Consorzio per i Sistemi a Grande Interfase" (CSGI) and by Progetto Finalizzato MSTA II of Italian CNR.

References and Notes

(1) Baurlein, P.; Herr, R.; Kloss, M.; Kumpers, J.; Maul, M.; Meissner, E. *J. Power Sources* **1999**, *82*, 585.

(2) Rodriguez Carvajal, J.; Rousse, G.; Masquelier, C.; Hervieu, M. *Phys. Rev. Lett.* **1998**, *81*, 4660.

(3) Massarotti, V.; Capsoni, D.; Bini, M.; Scardi, P.; Leoni, M.; Baron, V.; Berg, H. *J. Appl. Crystallogr.* **1999**, *32*, 1186.

(4) Azzoni, C. B.; Mozzati, M. C.; Paleari, A.; Massarotti, V.; Bini, M.; Capsoni, D. *Z. Naturforsch.* **1998**, *53a*, 771.

(5) Massarotti, V.; Capsoni, D.; Bini, M.; Chiodelli, G.; Azzoni, C. B.; Mozzati, M. C.; Paleari, A. *J. Solid State Chem.* **1997**, *131*, 94.

(6) Capsoni, D.; Bini, M.; Chiodelli, G.; Massarotti, V.; Azzoni, C. B.; Mozzati, M. C.; Comin, A. *Phys. Chem. Chem. Phys.* **2001**, *3*, 2162.

(7) Yoshio, M.; Noguchi, H.; Todorov, Y.; Hideshima, Y. *Denki Kagaku* **1998**, *66*, 1198.

(8) Rodriguez-Carvajal, J. *Physica B* **1993**, *192*, 55.

(9) Azzoni, C. B.; Mozzati, M. C.; Paleari, A.; Bini, M.; Capsoni, D.; Chiodelli, G.; Massarotti, V. *Z. Naturforsch.* **1999**, *54a*, 579.

(10) Mustarelli, P.; Massarotti, V.; Bini, M.; Capsoni, D. *Phys. Rev. B* **1997**, *55*, 10218.

(11) Lee, Y. J., Wang, F.; Grey, C. P. *J. Am. Chem. Soc*. **1998**, *120*, 12601.

(12) Nayeem, A.; Yesinowski, J. P. *J. Chem. Phys.* **1988**, *89*, 4600.

(13) Massiot, D.; Vosegaard, T.; Magneron, N.; Trumeau, D.; Montouillot, V.; Berthet, P.; Loiseau, T.; Bujoli, B. *Solid State NMR* **1999**, *15*, 159.

(14) Massarotti, V.; Capsoni, D.; Bini, M.; Azzoni, C. B.; Paleari, A. *J. Solid State Chem.* **1997**, *128*, 80.

(15) Berg, H.; Thomas, J. O.; Liu, W.; Farrington, G. C. *Solid State Ionics* **1998**, *112*, 165.

(16) Bellitto, C.; DiMarco, M. G.; Branford, W. R.; Green, M. A.; Neumann, D. A. *Solid State Ionics* **2001**, *140*, 77.

(17) Verhoeven, V. W. J.; de Schepper, I. M.; Nachtgaal, G.; Kentgens, A. P. M.; Kelder, E. M.; Schoonman, J.; Mulder, F. M. *Phys. Rev. Lett.* **2001**, *86*, 4314.

(18) Ammundsen, B.; Jones, D. J.; Roziere, J.; Villain, F. *J. Phys. Chem. B*, **1998**, *102*, 7939.

(19) Oikawa, K.; Kamiyama, T.; Izumi, F.; Nakazato, D.; Ikuta, H.; Wakihara, M. *J. Solid State Chem.* **1999**, *146*, 322.

(20) Aitchison, P.; Ammundsen, B.; Jones, D. J.; Burns, G.; Roziere, J. *J. Mater. Chem.* **1999**, *9*, 3125.

(21) Masquelier, C.; Tabuchi, M.; Ado, K.; Kanno, R.; Kobayashi, Y.; Maki, Y.; Nakamura, O.; Goodenough, J. B. *J. Solid State Chem.* **1996**, *123*, 255.